
01 Mar 2023

Engineering Oxygen Vacancy-Rich CeO_x overcoating Onto Ni/ Al₂O₃ by Atomic Layer Deposition for Bi-Reforming of Methane

Baitang Jin

Kaiying Wang

Han Yu

Xiaoqing He

et. al. For a complete list of authors, see https://scholarsmine.mst.edu/che_bioeng_facwork/1244

Follow this and additional works at: https://scholarsmine.mst.edu/che_bioeng_facwork



Part of the [Biochemical and Biomolecular Engineering Commons](#)

Recommended Citation

B. Jin et al., "Engineering Oxygen Vacancy-Rich CeO_x overcoating Onto Ni/Al₂O₃ by Atomic Layer Deposition for Bi-Reforming of Methane," *Chemical Engineering Journal*, vol. 459, article no. 141611, Elsevier, Mar 2023.

The definitive version is available at <https://doi.org/10.1016/j.cej.2023.141611>

This Article - Journal is brought to you for free and open access by Scholars' Mine. It has been accepted for inclusion in Chemical and Biochemical Engineering Faculty Research & Creative Works by an authorized administrator of Scholars' Mine. This work is protected by U. S. Copyright Law. Unauthorized use including reproduction for redistribution requires the permission of the copyright holder. For more information, please contact scholarsmine@mst.edu.



Engineering oxygen vacancy-rich CeO_x overcoating onto Ni/Al₂O₃ by atomic layer deposition for bi-reforming of methane

Baitang Jin^a, Kaiying Wang^b, Han Yu^a, Xiaoqing He^{c,d}, Xinhua Liang^{a,b,*}

^a Linda and Bipin Doshi Department of Chemical and Biochemical Engineering, Missouri University of Science and Technology, Rolla, MO 65409, United States

^b Department of Energy, Environmental and Chemical Engineering, Washington University in St. Louis, St. Louis, MO 63130, United States

^c Electron Microscopy Core Facility, University of Missouri, Columbia, MO 65211, United States

^d Department of Mechanical and Aerospace Engineering, University of Missouri, Columbia, MO 65211, United States

ARTICLE INFO

Keywords:

Non-stoichiometric CeO_x
Atomic layer deposition (ALD)
Bi-reforming of methane (BRM)
Oxygen vacancy

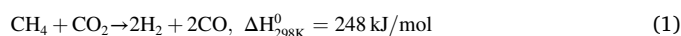
ABSTRACT

Atomic layer deposition (ALD) was applied to develop CeO_x-overcoated Ni/Al₂O₃ catalyst for bi-reforming of methane (BRM), as the combination of dry reforming of methane (DRM) and steam reforming of methane (SRM). Non-stoichiometric CeO_x thin films were successfully deposited on Ni/Al₂O₃ particles by ALD, which constructed a beneficial Ni-CeO_x interface and modified the catalyst property. Ascribed to the unique ALD growth mode, a high amount of Ce(III) and oxygen vacancies existed in the ALD-deposited CeO_x overcoating. A reduction process before the BRM reaction contributed to the further reduction of Ce(IV) to Ce(III), resulting in more oxygen vacancies. The oxygen vacancies at the Ni-CeO_x interface enabled a high rate of CO₂ activation and enabled the balance between the activation of CO₂ and H₂O for BRM. Due to its oxygen vacancies as activation sites for CO₂ and H₂O, CeO_x ALD overcoating significantly improved the activity of Ni/Al₂O₃ catalyst and achieved a better control in the H₂/CO ratio with a suitable ratio of H₂O/CO₂/CH₄ feed. CeO_x overcoatings enhanced the reducibility of Ni(II) sites and assisted in preventing Ni from oxidation during the BRM reaction. Less carbon deposition was achieved by the Ni/Al₂O₃ catalyst with CeO_x overcoating as ascribed to its better reactant activation capacity.

1. Introduction

With the rising greenhouse gas (GHG) emissions, the net-zero target by 2050 set in the Paris Agreement and Conference of the Parties necessitates a technically feasible strategy to chemically recycle captured CO₂ into value-added products for the decarbonization roadmap [1,2]. Dry reforming of methane (DRM, eq. (1)) exhibits remarkable potential in consuming the GHG (i.e., CH₄ and CO₂), utilizing the off-peak energy, and producing syngas (i.e., H₂ and CO) with H₂/CO molar ratio of ~ 1 as industrial C1-block, whereas the current steam reforming of methane (SRM, eq. (2), with H₂/CO molar ratio of ~ 3) faces high H₂/CO ratio with the formation of side-product CO₂ [3]. Without reconstructing the present infrastructure, bi-reforming of methane (BRM), which incorporates DRM into SRM, can achieve industrial utilization of CO₂ and production of valuable syngas with desired H₂/CO ratio [1,3,4]. Especially, syngas with an H₂/CO molar ratio of ~ 2 (metgas) can be achieved (eq. (3)) by BRM and it is optimal for the production of methanol

and dimethyl ether, which are blueprinted as the renewable CO₂-recycling synthetic fuels to substitute the conventional fossil fuels in the near future [3,5–7]. Nickel, with low cost and high reactivity for CH₄, has been widely investigated as methane reforming catalysts [1,8,9]. However, Ni-based catalysts face the challenge of sintering and coking. Especially, the side reactions (e.g., CH₄ cracking and Boudouard reactions) result in carbon growth and high pressure drop in fixed bed reactors [10–12]. To inhibit carbon growth and accumulation, constructing a metal-oxide interface (e.g., introducing promoter or overcoating) and enhancing the concentration of interfacial oxygen surrounding Ni sites can kinetically accelerate the removal rate of carbon intermediates via CO₂ oxidation [13].



* Corresponding author at: Department of Energy, Environmental and Chemical Engineering, Washington University in St. Louis, St. Louis, MO 63130, United States.

E-mail address: xinhua.liang@wustl.edu (X. Liang).

<https://doi.org/10.1016/j.cej.2023.141611>

Received 31 October 2022; Received in revised form 3 January 2023; Accepted 26 January 2023

Available online 30 January 2023

1385-8947/© 2023 Elsevier B.V. All rights reserved.



CeO_2 , with reversible valence states and oxygen vacancies, has been proven to be effective to provide active O sites and enhance the performance of catalysts for methane reforming [14]. The intimate contact between Ni and CeO_2 exhibits a strong influence on the catalytic behavior. For instance, Yan et. al utilized plasma-synthesized Ni/ CeO_2 - SiO_2 with closer Ni- CeO_2 contact than that of the catalyst prepared by the calcination method for DRM, and achieved better activity and stability due to the more reactive O species at Ni- CeO_2 interface [8]. Besides, the morphology of CeO_2 (e.g., nanorod, nanoparticles, or thin-film) has been reported to play a decisive role on the concentration of oxygen vacancies [15–18], which can participate in CO_2 activation [19]. To develop a highly active and stable catalyst for methane reforming, it is desirable to deposit CeO_x with high concentration of oxygen vacancies and construct a sufficient metal-oxide interface.

Atomic layer deposition (ALD) is a gas phase self-limiting thin film coating technology based on cycle-repeatedly sequential surface reactions [20]. With a desired number of ALD cycles, the layer-by-layer growth could be achieved at the atomic level. For heterogeneous catalysts, ALD has been applied to prepare highly dispersed metal clusters as the active catalytic sites, from single atoms to nm-scale nanoparticles (NPs) [20–23]; ALD can also synthesize ultrathin oxide layer or overcoating, which exhibits unique features in generating additional active sites [21,24], blocking the undesired sites [25], or constructing functional structure [25,26] for heterogeneous catalysts. Studies showed that the encapsulating structure of ALD oxide film became discontinuous and partially encapsulating on the active metal sites after high-temperature treatment, which effectively exposed the active metal sites and created desirable metal-oxide interfaces [25,27–29]. Ascribed to the growth mode of ALD, studies showed that the composition of ALD oxide thin film could be non-stoichiometric and exhibited unique properties, which differs from the oxides prepared by traditional methods [24,29,30]. Considering the importance of interfacial oxygen species, depositing a suitable oxide onto Ni/ Al_2O_3 catalyst as overcoating can effectively construct an ideal metal-oxide interface and tune the catalytic performance. In this work, a highly active and coke-resistant CeO_x -Ni/ Al_2O_3 catalyst was synthesized by Ni ALD on Al_2O_3 support, followed by CeO_x ALD. CeO_x ALD exhibited unique properties and enhanced the catalytic performance of Ni/ Al_2O_3 , enabling to tune the H_2/CO ratio for the BRM reaction.

2. Experimental

2.1. Catalyst preparation

Ni/ Al_2O_3 catalyst was synthesized by depositing Ni NPs onto α - Al_2O_3 NPs (Alfa Aesar, 99+%, 80 nm, US3008) using ALD in a home-made fluidized bed reactor [31], as shown in Fig. S1. Bis(cyclopentadienyl) nickel (NiCp_2 , Alfa Aesar) and hydrogen (Airgas, 99.99 %) were used as precursors, and N_2 (Airgas, 99.99 %) was used as a carrier gas or flush gas. Before ALD, α - Al_2O_3 NPs were loaded in the reactor and preheated at 150 °C overnight to remove moisture. Then, the reactor temperature was set at 300 °C for Ni ALD. For a typical Ni ALD cycle, NiCp_2 was dosed into the ALD reactor by heating a NiCp_2 bubbler at 90 °C and delivering the vaporized NiCp_2 with 6 mL/min N_2 for 300 s to initiate the first half-reaction. The ALD reactor was flushed by N_2 flush for 600 s to remove excess NiCp_2 and by-products, followed by vacuum evacuation for 20 s. For the second half-reaction, 20 mL/min H_2 was dosed into the reactor for 300 s to react with the chemisorbed NiCp_2 and generate Ni NPs, followed by the clean-up using N_2 flush and evacuation. In this work, 5 cycles of Ni ALD were applied to synthesize Ni NPs and the catalyst was labeled as Ni/ Al_2O_3 .

CeO_x ALD was conducted to deposit CeO_x overcoating onto the Ni/ Al_2O_3 catalyst in the same ALD reactor. Tris(i-propylcyclopentadienyl) cerium ($\text{Ce}(\text{iPrCp})_3$, Strem Chemicals, 99.9 %) and deionized water

were used as the precursors for CeO_x ALD and N_2 was used as a carrier gas. The reactor temperature was set at 200 °C. For a typical CeO_x ALD cycle, $\text{Ce}(\text{iPrCp})_3$ was dosed into the reactor by heating a $\text{Ce}(\text{iPrCp})_3$ bubbler at 150 °C and delivering the vaporized $\text{Ce}(\text{iPrCp})_3$ with 15 mL/min N_2 for 60 s, followed by the reactor clean-up using N_2 flush and evacuation. Then, H_2O was dosed into the reactor for 60 s to react with the chemisorbed $\text{Ce}(\text{iPrCp})_3$ and generate the CeO_x overcoating, followed by inert gas flush and vacuum evacuation process. In this work, 10, 30, 60, and 90 cycles of CeO_x ALD were applied on the Ni/ Al_2O_3 catalyst, and the catalyst was labeled as 10 CeO_x -Ni/ Al_2O_3 , 30 CeO_x -Ni/ Al_2O_3 , 60 CeO_x -Ni/ Al_2O_3 , and 90 CeO_x -Ni/ Al_2O_3 , respectively. For ease of characterization, 200 cycles of CeO_x ALD were applied on Ni/ Al_2O_3 and the catalyst was labeled as CeO_x -Ni/ Al_2O_3 .

For comparison, Al_2O_3 ALD was conducted to deposit Al_2O_3 overcoating onto the Ni/ Al_2O_3 catalyst in the same reactor. Trimethylaluminum (TMA, Sigma-Aldrich) and deionized water were used as the precursors for Al_2O_3 ALD and N_2 was used as the carrier gas. The ALD reaction temperature was 150 °C for Al_2O_3 ALD. For a typical Al_2O_3 ALD cycle, TMA was dosed into the reactor for 300 s, followed by the reactor clean-up using N_2 flush and evacuation. Then, H_2O was dosed into the reactor for 300 s to react with the chemisorbed TMA and generate Al_2O_3 thin film, followed by the reactor clean-up process. 10 cycles of Al_2O_3 ALD were applied to achieve the similar thickness of CeO_x thin film on 60 CeO_x -Ni/ Al_2O_3 based the ALD thin film growth rates. The catalyst was labeled as Al_2O_3 -Ni/ Al_2O_3 .

For comparison, liquid-based incipient wetness method was conducted to deposit CeO_2 as a promoter onto the Ni/ Al_2O_3 catalyst. Ni/ Al_2O_3 particles were impregnated in an aqueous solution of $\text{Ce}(\text{NO}_3)_3$ (Alfa Aesar, 99.99 %) for 1 h (with a similar amount of CeO_x on 60 CeO_x -Ni/ Al_2O_3), dried at 100 °C in an oven, and then calcinated in the air in a tubular furnace at 500 °C for 3 h. The catalyst was labeled as iw CeO_2 /Ni/ Al_2O_3 .

2.2. Bi-reforming of methane reaction

A home-made fixed bed reactor system was built for bi-reforming of methane reaction, as shown in Fig. S2. The reactant control and delivery system were achieved by mass flow controllers (MKS Instruments) for controlling gas flow rates and a syringe pump (Chemyx Fusion 101) for controlling water flow rate. To ensure the gasification of water, heating tapes (Omega Engineering) were used to heat up the water feeding line to 120 °C. A quartz tube with an inner diameter of 10 mm was used as a reactor, which was placed vertically and heated by a tubular furnace (Carbolite Gero, Ltd.). A K-type thermocouple (Omega Engineering) was positioned right above the catalyst bed to monitor the reactor temperature. One on-line gas chromatograph (SRI 8610C) was used to analyze the products, with a 6-foot Hayesep D column and TCD detector. A cold trap tank was used to condense any by-product water from the product gas before it entered into the GC.

For the BRM reaction, ~50 mg catalyst particles were loaded on ~30 mg quartz wool in the quartz tube reactor. A reduction procedure was conducted at 800 °C for 1 h using 20 % H_2 /80 %Ar (v/v%) mixture with a flow rate of 100 mL/min. After reduction, the temperature was set at a desired temperature and the reactant gases (i.e., CH_4 , CO_2 , and gas-phase H_2O) were introduced into the reactor.

2.3. Catalyst characterizations

Transmission electron microscopy (TEM) was conducted using a probe-aberration corrected ThermoFisher Spectra 300 TEM with 4-quadrant Super-X EDS detectors to measure the Ni particle size and acquire the morphology of the catalysts. X-ray photoelectron spectroscopy (XPS) was conducted using a Kratos Axis 165 X-ray photoelectron spectrometer to determine the chemical states of different elements. XRD was conducted on an X-Pert Multi-purpose diffractometer to access the phase information of the catalysts.

H₂-temperature programmed reduction (H₂-TPR) was conducted using a Micromeritics AutoChem II 2920 instrument. The catalysts were first pretreated in Ar at 300 °C for 1 h. Then, H₂-TPR was performed using 10 %H₂/90 %Ar (v/v%) from 50 to 900 °C with a temperature increasing rate of 10 °C/min. The H₂ pulse chemisorption experiment was also conducted on this Micromeritics AutoChem II 2920 instrument. The sample was first pretreated in a H₂/Ar (mixed at 10/90 vol%) flow for 1 h and flushed in Ar for 1 h at 700 °C. After cooling down to 50 °C in Ar, the samples underwent the cycles of H₂/Ar pulse and Ar pulse.

Thermogravimetric analysis (TGA) was conducted using a TA Instrument Q50 analyzer. The sample underwent a temperature ramping from room temperature to 200 °C, holding at 200 °C for 1 h, and temperature ramping from 200 to 800 °C at 10 °C/min in 40 mL/min Ar.

CO₂-temperature programmed desorption (CO₂-TPD) and O₂-temperature programmed oxidation (O₂-TPO) were conducted using the methane reforming reactor. A mass spectrometer (Stanford Research System, QMS 200) with a pressure-time mode was used to detect and record the gas signal. The m/e value of the MS signal was taken to identify the gas species (e.g., 40 for Ar, 28 for CO, 44 for CO₂, and 32 for O₂). For CO₂-TPD, the catalyst was first reduced at 800 °C using H₂, then CO₂ saturation in 20 mL/min 20 %CO₂/80 %Ar (v/v%) mixture for 1 h at 80 °C and Ar flush in 20 mL/min Ar for 1 h at 80 °C. After this pretreatment, CO₂-TPO was performed in Ar, starting from 80 to 700 °C with a temperature increasing rate of 10 °C/min. For O₂-TPO, the spent catalysts were first pretreated in Ar at 100 °C for 1 h and then oxidized in 20 %O₂/80 %Ar (v/v%) from 100 to 800 °C.

3. Results and discussion

3.1. Material characterizations

TEM was conducted to determine the morphology of the Ni/Al₂O₃ and 60CeO_x-Ni/Al₂O₃ catalysts. As shown in Fig. 1a, the average size of Ni NPs (in oxidized state) on the ALD-prepared Ni/Al₂O₃ was 2.7 ± 0.9 nm, which is much smaller than those prepared by the traditional incipient wetness method. After 60 cycles of CeO_x ALD, the average size of Ni NPs (in oxidized state) on 60CeO_x-Ni/Al₂O₃ was about 2.9 ± 1.0 nm

nm, which was almost the same as that of the pristine Ni/Al₂O₃. Since the CeO_x ALD process was conducted at a mild temperature of 200 °C, there was no obvious sintering of Ni NPs during the CeO₂ ALD coating process. For the reduced catalysts, the average size of the reduced Ni/Al₂O₃ catalyst is 9.7 ± 2.3 nm and the average size of the reduced 60CeO_x-Ni/Al₂O₃ catalyst is 6.2 ± 1.5 nm, which indicates the CeO_x overcoating inhibited the sintering of the Ni during the high-temperature reduction process. As a bottom-up synthesis strategy, ALD can create an ultra-thin CeO_x overcoating on Ni/Al₂O₃ surface conformally and help prevent sintering. The lattice spacing of 0.203 nm could be observed with the HRTEM analysis, which was ascribed to the (111) of metallic Ni. The element mapping result in Fig. 1f exhibited the uniform distribution of CeO_x overcoating on both Ni and Al₂O₃, which confirms the Ni-CeO_x interface. In addition, XRD was conducted to determine the phase structure of Ni/Al₂O₃ and CeO_x-Ni/Al₂O₃, as shown in Fig. S3. It could be seen that the main peaks were assigned to α-Al₂O₃, with a small amount of NiO. The peaks assigned to any cerium oxide could be hardly seen, probably due to the low loading or the amorphous structure.

To examine the property of CeO_x thin films prepared by ALD, XPS was conducted on the fresh and reduced ALD-prepared CeO_x-Ni/Al₂O₃ and iwCeO₂-Ni/Al₂O₃ catalysts in Fig. 2 and Fig. S4. All spectra were calibrated by fixing adventitious carbon at 284.5 eV (C1s in Fig. S4). For the Ce element in Fig. 2a, the Ce(IV) peaks included v at 882.3 eV, v' at 886.7 eV, v'' at 897.8 eV, u at 899.3 eV, u' at 903.5 eV, and u'' at 916.4 eV [32,33]. The Ce(III) peaks included v₀ at 880.8 eV, v' at 885.2 eV, u₀ at 899.3 eV, and u' at 903.5 eV [32,33]. To have a quantitative comparison, the Ce(III) contents were calculated from the (v₀ + v' + u₀ + u')% for the ALD-prepared and IW-prepared catalysts. Besides, the characteristic u'' peak, without any overlapping with other peaks, could represent the relative Ce(IV) content and was used to indicate the Ce(IV) amount. The Ce(III) content of the fresh ALD-prepared CeO_x-Ni/Al₂O₃ was 38.0 %, with u'' peak as Ce(IV) representative at 4.7 %. Based on the Ce 3d results, there was more Ce(III) in the ALD-prepared CeO_x-Ni/Al₂O₃ catalyst. For cerium oxide, the content of Ce(III) is generally considered a significant indicator of the oxygen storage capacity, which assists the surface reaction and enhances the catalytic

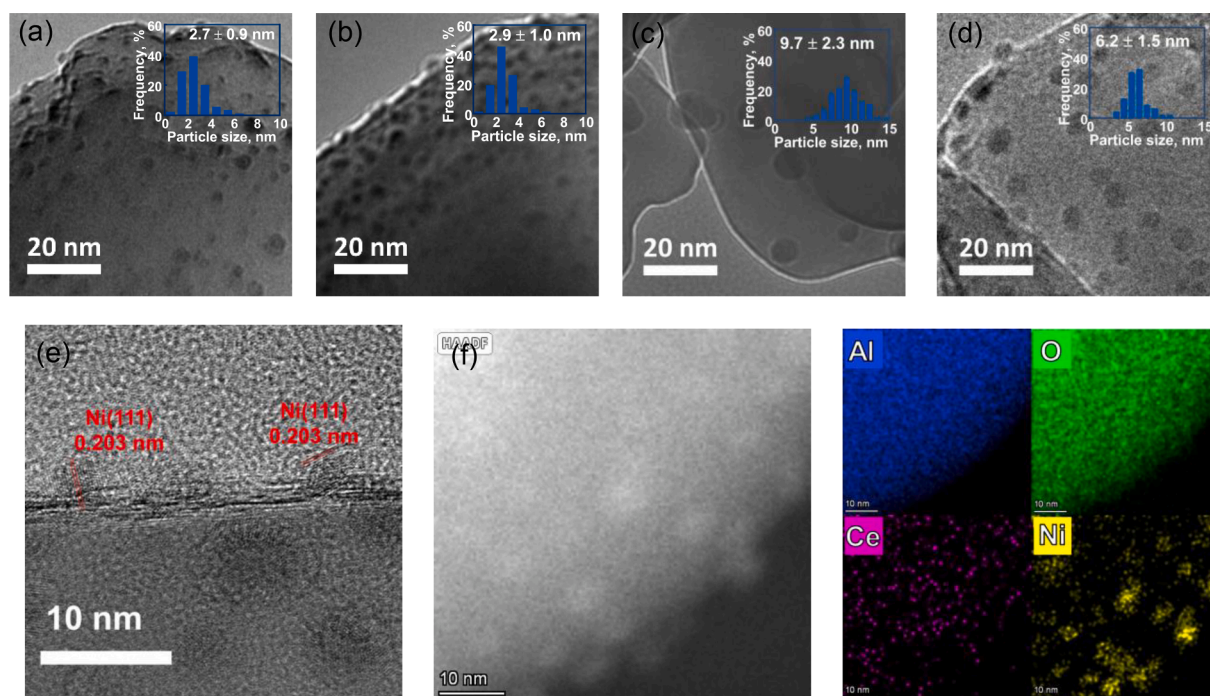


Fig. 1. TEM images of (a) fresh Ni/Al₂O₃, (b) fresh 60CeO_x-Ni/Al₂O₃, (c) reduced Ni/Al₂O₃, and (d-f) reduced 60CeO_x-Ni/Al₂O₃. (f) EDS elemental mapping of Al, O, Ce, and Ni for reduced 60CeO_x-Ni/Al₂O₃. The inset images show the size distribution of Ni NPs.

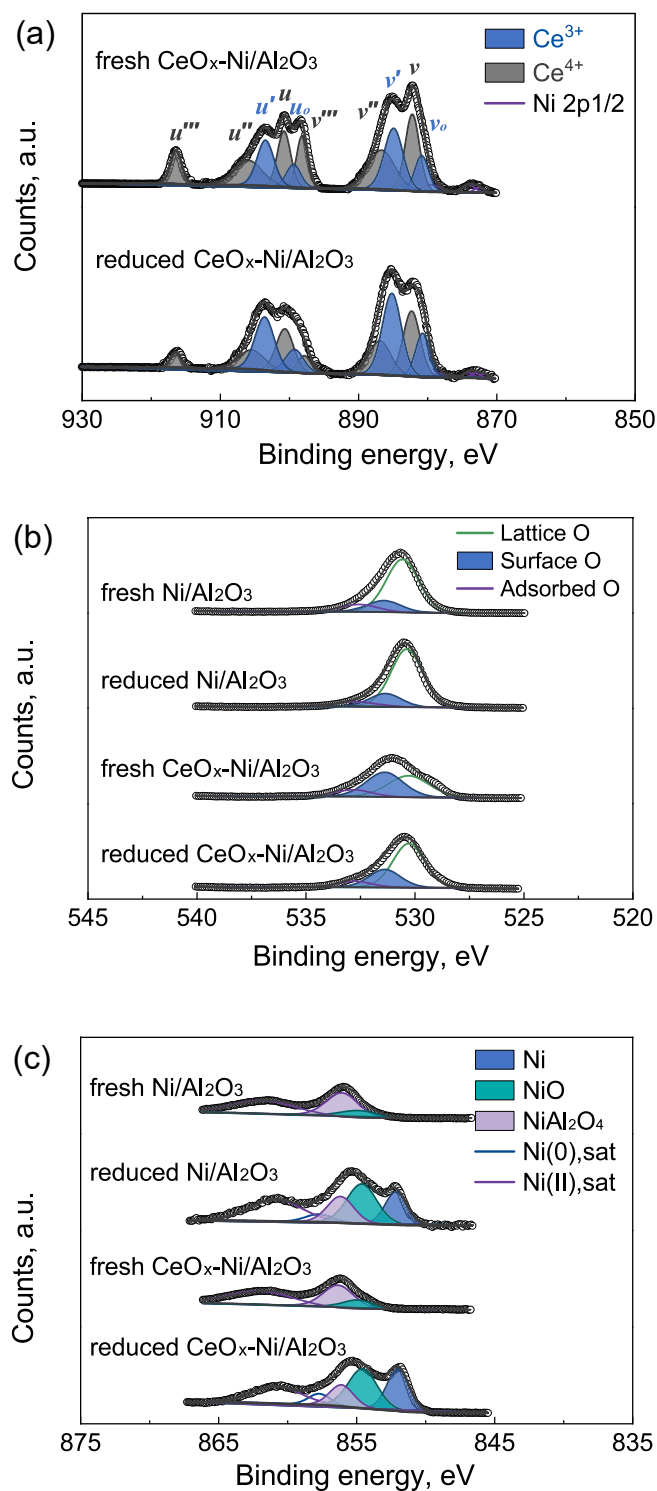


Fig. 2. XPS spectra of (a) Ce3d for fresh $\text{CeO}_x\text{-Ni/Al}_2\text{O}_3$ and reduced $\text{CeO}_x\text{-Ni/Al}_2\text{O}_3$, (b) O 1s, and (c) Ni 2p $_{3/2}$ for fresh $\text{Ni/Al}_2\text{O}_3$, reduced $\text{Ni/Al}_2\text{O}_3$, fresh $\text{CeO}_x\text{-Ni/Al}_2\text{O}_3$, and reduced $\text{CeO}_x\text{-Ni/Al}_2\text{O}_3$.

activity [33]. For the ALD-prepared catalyst, the higher amount of Ce (III) should be ascribed to the unique ALD growth mode, because Ce (iPrCp) $_3$ and H $_2$ O would react to form Ce(OH) $_3$ initially, and the ultrathin film structure could favor the existence of Ce(III) [34–36]. Therefore, the ALD-prepared CeO_x overcoating had more Ce(III) than that prepared by the traditional liquid method and could participate in the surface reaction during methane reforming. During the H $_2$ -reduction process, the chemical states of Ce in Fig. 2a and O in Fig. 2b also

significantly changed. In the spectrum of Ce 3d, there was a higher Ce (III) content for $\text{CeO}_x\text{-Ni/Al}_2\text{O}_3$, with the Ce(III) ratio of 50.8 % based on ($v_0 + v'' + u_0 + u''$)% and the diagnostic peak (u'''') of 1.9 % for Ce(IV). For the IW-prepared $\text{iwCeO}_2\text{/Ni/Al}_2\text{O}_3$ catalyst, the fresh catalyst had a Ce (III) content at 22.4 % and u'''' peak as Ce(IV) representative at 6.4 %. After reduction, the reduced catalyst had a Ce(III)% content of 42.7 % and u'''' of 4.6 % for the $\text{iwCeO}_2\text{/Ni/Al}_2\text{O}_3$ catalyst. Compared with the spectra of the fresh $\text{CeO}_x\text{-Ni/Al}_2\text{O}_3$ catalysts with Ce(III)% of 40.0 % and u'''' of 4.8 %, the Ce(III) content for the reduced catalyst was higher, indicating the reduction of Ce(IV). Owing to the variable valences of Ce(III) and Ce(IV), Ce(IV) was reduced to Ce(III) during H $_2$ -reduction, and more oxygen vacancies were generated to keep the electronic balance of Ce(III) [18,41].

The oxygen species were investigated using XPS for $\text{Ni/Al}_2\text{O}_3$, ALD-overcoated $\text{CeO}_x\text{-Ni/Al}_2\text{O}_3$, ALD-overcoated $\text{Al}_2\text{O}_3\text{-Ni/Al}_2\text{O}_3$, and IW-promoted $\text{iwCeO}_2\text{/Ni/Al}_2\text{O}_3$. The O species were deconvoluted to three peaks, including the lattice O at ~ 530.5 eV for O of the metal oxide, the surface O at ~ 531.5 eV for low coordinated oxygen atoms, and the adsorbed O at ~ 532.7 eV from adsorbed H $_2$ O [37]. Especially, the surface oxygen consists of hydroxyl oxygen and deficient oxygen sites, which are important surface species. As shown in Fig. 2b, the content of surface O in $\text{Ni/Al}_2\text{O}_3$ was about ~ 15 %, which was smaller than ~ 45 % of the $\text{CeO}_x\text{-Ni/Al}_2\text{O}_3$ catalyst. For comparison, the content of surface O for the ALD-overcoated $\text{Al}_2\text{O}_3\text{-Ni/Al}_2\text{O}_3$ catalyst reached ~ 54 % and the content of surface O for IW-promoted $\text{iwCeO}_2\text{/Ni/Al}_2\text{O}_3$ reached ~ 23 % in Fig. S4. For the ALD-overcoated catalysts, the high content of the surface O indicated a large number of hydroxyls, regardless of CeO_x ALD or Al_2O_3 ALD overcoating. Besides, the higher content of surface O in the $\text{iwCeO}_2\text{/Ni/Al}_2\text{O}_3$ catalyst indicated that the CeO_2 promoter also increased the surface O for $\text{Ni/Al}_2\text{O}_3$ and didn't decrease after high temperature reduction, which was ascribed to the oxygen vacancies with $\text{Ce}^{4+}/\text{Ce}^{3+}$. Therefore, the surface O of the ALD-overcoated $\text{CeO}_x\text{-Ni/Al}_2\text{O}_3$ resulted from both the hydroxyl groups and oxygen vacancies. For O 1s of the samples after reduction, the surface O for ALD-overcoated $\text{CeO}_x\text{-Ni/Al}_2\text{O}_3$ was about 26.4 %, which was higher than 17.2 % for $\text{Ni/Al}_2\text{O}_3$, 20.1 % for $\text{Al}_2\text{O}_3\text{-Ni/Al}_2\text{O}_3$, and 21.0 % for $\text{iwCeO}_2\text{/Ni/Al}_2\text{O}_3$. For the ALD-overcoating catalysts (i.e., $\text{CeO}_x\text{-Ni/Al}_2\text{O}_3$ and $\text{Al}_2\text{O}_3\text{-Ni/Al}_2\text{O}_3$), the surface O significantly decreased after high-temperature reduction, which was ascribed to the removal of hydroxyl groups at high temperature, whereas the $\text{CeO}_x\text{-Ni/Al}_2\text{O}_3$ catalyst still had a high amount of surface oxygen. Comparing $\text{CeO}_x\text{-Ni/Al}_2\text{O}_3$ and $\text{Al}_2\text{O}_3\text{-Ni/Al}_2\text{O}_3$, the higher surface O of $\text{CeO}_x\text{-Ni/Al}_2\text{O}_3$ should result from the oxygen vacancies. The higher amount of oxygen vacancies after reduction for reduced $\text{CeO}_x\text{-Ni/Al}_2\text{O}_3$ was also confirmed by the spectra of Ce 3d. For the bi-reforming of methane, the high amount of oxygen vacancies could serve as the activation sites for CO $_2$ and enhance the catalytic performance.

Fig. 2 and Fig. S4 depict the XPS spectra for the reduced $\text{Ni/Al}_2\text{O}_3$, reduced $\text{CeO}_x\text{-Ni/Al}_2\text{O}_3$, reduced $\text{Al}_2\text{O}_3\text{-Ni/Al}_2\text{O}_3$, and reduced $\text{iwCeO}_2\text{/Ni/Al}_2\text{O}_3$ catalysts. For Ni 2p $_{3/2}$, the peaks could be deconvoluted into different Ni species as metallic Ni at ~ 852.1 eV, NiO at ~ 854.5 eV, NiAl $_2$ O $_4$ at ~ 856.2 eV, and satellite peaks due to shake-up phenomena, including Ni(0),sat at ~ 857.8 eV and Ni(II),sat at ~ 860.8 eV [38,39]. Especially, the spinel NiAl $_2$ O $_4$ was highly thermal stable with a reduction temperature of ~ 800 °C, whereas NiO was easily reduced to Ni at high temperatures and highly reductive DRM reaction conditions. For the fresh catalyst (Fig. S4), a high amount of NiAl $_2$ O $_4$ indicates that the interaction between NiO and Al_2O_3 for ALD-prepared $\text{Ni/Al}_2\text{O}_3$ was very strong, which was due to the chemisorption-based growth mechanism [40]. Under this circumstance, the presence of NiAl $_2$ O $_4$ after reduction treatment could be considered an incomplete reduction, which could lead to the activity loss. Comparing the different catalysts after reduction in Fig. 2c and Fig. S4e, the content of NiAl $_2$ O $_4$ was 17.6 % for $\text{Ni/Al}_2\text{O}_3$, 13.8 % for $\text{CeO}_x\text{-Ni/Al}_2\text{O}_3$, 26.4 % for $\text{Al}_2\text{O}_3\text{-Ni/Al}_2\text{O}_3$, and 14.1 % for $\text{iwCeO}_2\text{/Ni/Al}_2\text{O}_3$. Based on the chemical states of Ni, the CeO_x ALD overcoating, or CeO_2 IW promoter significantly enhanced the

reducibility, whereas the Al_2O_3 ALD overcoating exhibited a negative effect on the reducibility due to the formation of NiAl_2O_4 . In this case, CeO_x ALD effectively weakened the metal-support interaction (i.e., Ni- Al_2O_3 interaction) and released more Ni from NiAl_2O_4 , while Al_2O_3 ALD overcoating resulted in the formation of more NiAl_2O_4 .

To characterize the metal-support interactions and probe the effects of CeO_x ALD thin film, H_2 -TPR was conducted for Ni/ Al_2O_3 , ALD-overcoated 60 CeO_x -Ni/ Al_2O_3 , ALD-overcoated Al_2O_3 -Ni/ Al_2O_3 , and IW-promoted iw CeO_2 /Ni/ Al_2O_3 , as shown in Fig. 3. Depending on the extent of Ni diffusion into the Al_2O_3 lattice, a higher reduction temperature is necessary for the species with a greater extent of diffusion/interaction and various species can be identified by TPR [42], including free NiO without any interaction, NiO- Al_2O_3 with interaction, and NiAl_2O_4 with spinel crystallization [40,42]. For Ni/ Al_2O_3 , the dominant peak at $\sim 340^\circ\text{C}$ was assigned to NiO, the peak at $\sim 515^\circ\text{C}$ was assigned to NiO- Al_2O_3 , and the peak $>700^\circ\text{C}$ was assigned to NiAl_2O_4 . Therefore, Ni(II) peaks in Ni/ Al_2O_3 mainly consisted of free NiO and NiO- Al_2O_3 , with a reduction degree at 72 %. For ALD-overcoated 60 CeO_x -Ni/ Al_2O_3 , the NiO peak was at $\sim 280^\circ\text{C}$ and the NiO- Al_2O_3 peak was at $\sim 520^\circ\text{C}$. Clearly, CeO_x ALD facilitated the reduction process of the free NiO sites because the free NiO shifted to a lower temperature. The reduction degree for the 60 CeO_x -Ni/ Al_2O_3 was about 77 %, indicating that the CeO_x ALD promoted the reduction of Ni sites. For ALD-overcoated Ni/ Al_2O_3 , the NiO peak and the NiO- Al_2O_3 peak almost remained in the same position as those of Ni/ Al_2O_3 with similar reduction degree at 71 %, but the peaks became broadened, especially the NiO- Al_2O_3 peak, indicating that Al_2O_3 ALD films interacted with Ni sites. Regarding the reducibility, CeO_x ALD overcoating was beneficial to the catalytic activity as compared to Al_2O_3 as the overcoating material. As for iw CeO_2 /Ni/ Al_2O_3 , the overall peak was shifted to lower temperatures, including $\sim 320^\circ\text{C}$ for NiO and $\sim 470^\circ\text{C}$ for NiO- Al_2O_3 , with a reduction degree of 79 %. Especially, the promoting effect of IW CeO_2 on NiO- Al_2O_3 might arise from the interaction between NiO and CeO_2 , and the possible formation of NiO- CeO_2 after calcination, because the introduction of CeO_2 by the incipient wetness method requires a high temperature calcination at 500°C . The difference between ALD-overcoated CeO_x -Ni/ Al_2O_3 and IW-promoted iw CeO_2 /Ni/ Al_2O_3 could result from the morphology of ALD CeO_x films, because the role of CeO_x overcoating was prepared by surface modification instead of bulk transformation. Therefore, CeO_x ALD provided an efficient Ni- CeO_x interface and promoted the reducibility of Ni sites for the Ni/ Al_2O_3 catalyst.

Although the stoichiometry of the bi-reforming of methane can be realized by the combination of SRM and DRM, the competition between SRM and DRM reactions should be considered for practical application. Especially, the surface reaction competition between SRM and DRM can

be determined by the activation process of H_2O and CO_2 on the surface oxygen sites. To evaluate the surface oxygen and the CO_2 affinity, CO_2 temperature-program desorption (CO_2 -TPD) was performed. According to the desorption temperature, the basic sites can be classified as weak basic sites $< 200^\circ\text{C}$ for physical adsorption or Brønsted basic sites (e.g., $-\text{OH}$ group), medium basic sites at $200\text{--}350^\circ\text{C}$ for Lewis acid-base pair $\text{Ce}^{4+}\text{--O}^{2-}$, and strong basic sites $>350^\circ\text{C}$ for oxygen vacancies or oxygen defects [33,43]. As shown in Fig. 4, the peaks for the Ni/ Al_2O_3 catalyst mainly consisted of weak basic sites due to the acidic and $-\text{OH}$ -rich properties of Al_2O_3 . For the same reason, Al_2O_3 ALD failed to enhance the medium basic sites or strong basic sites of the catalyst. In contrast, the addition of CeO_2 enhanced both the medium basic sites and strong basic sites by IW or ALD method, because of the basic nature of CeO_2 . However, the ALD-deposited CeO_x exhibited stronger basic properties in terms of quantity and strength, and thus a higher CO_2 affinity than that of the IW-prepared CeO_2 . For iw CeO_2 /Ni/ Al_2O_3 , the introduction of CeO_2 by the IW method significantly increased the medium basic sites and provided a small amount of the strong basic sites. For 60 CeO_x -Ni/ Al_2O_3 , the deposition of CeO_x by ALD brought both medium basic sites and strong basic sites, especially for the strong basic sites. In comparison, the high amount of strong basic sites indicated there were more oxygen vacancies for the catalyst with CeO_x ALD overcoating. The high CO_2 affinities and special oxygen sites for CeO_x ALD overcoated catalyst should result from the thin-film structure and unique growth mode. It has been reported that the oxygen vacancies of CeO_2 can be tuned by its morphology and structure and a thin film structure enabled the high amount of oxygen vacancies [15–18]. As ascribed to the layer growth mode of ALD thin films [36], the Ni/ Al_2O_3 catalyst with CeO_x ALD overcoating would have enhanced catalytic activity due to the oxygen vacancies of CeO_x .

3.2. Catalytic performance for bi-reforming of methane

The equilibrium of bi-reforming of methane by co-feeding CH_4 , H_2O , and CO_2 was calculated using the Gibbs reactor and Soave-Redlich-Kwong equation of state in ChemCAD, as shown in Fig. S5. At varying temperatures, the equilibrium conversion of CH_4 was almost the same at all conditions, but the H_2/CO ratio was very different and varied with the feeding. Here, the H_2/CO ratio from the direct stoichiometric combination of SRM and DRM was used for the comparison with the equilibrium value (see Supporting Information). The difference between the direct stoichiometric value and the equilibrium value was mainly caused by the water-gas shift reaction or reverse water-gas shift reaction (WGS/RWGS). A higher temperature drives the equilibrium H_2/CO molar ratio towards 2, indicating a weaker effect of the WGS/RWGS at a

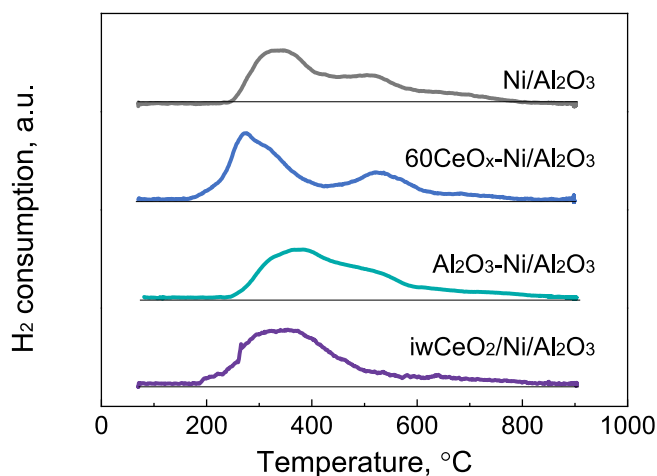


Fig. 3. H_2 -TPR spectra of Ni/ Al_2O_3 , 60 CeO_x -Ni/ Al_2O_3 , Al_2O_3 -Ni/ Al_2O_3 , and iw CeO_2 /Ni/ Al_2O_3 .

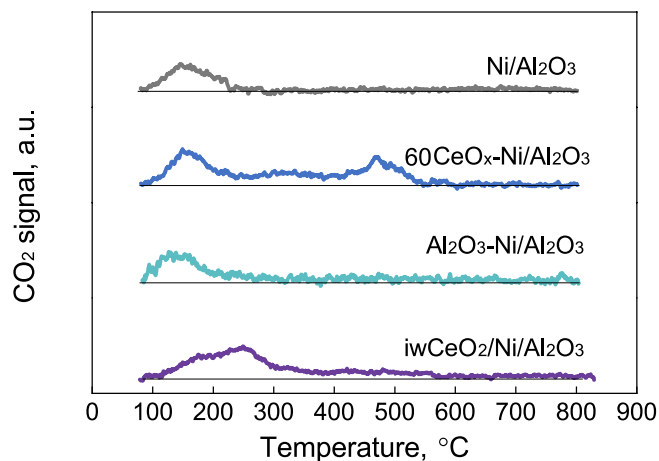


Fig. 4. CO_2 -TPD spectra of Ni/ Al_2O_3 , 60 CeO_x -Ni/ Al_2O_3 , Al_2O_3 -Ni/ Al_2O_3 , and iw CeO_2 /Ni/ Al_2O_3 .

higher temperature. Besides, the H_2/CO ratio exhibited a tunable ratio at varying inlet feed of CH_4 , H_2O , and CO_2 .

Bi-reforming of methane with $H_2O/CO_2/CH_4 = 2/1/3$ as a feedstock was conducted using the Ni/Al_2O_3 and ALD CeO_x -overcoated Ni/Al_2O_3 catalysts. Fig. 5a and 5b show the CH_4 conversion and H_2/CO for BRM reaction at $850^\circ C$. As shown in Fig. 5a, the CH_4 conversion of Ni/Al_2O_3 reached 61.9 % at the initial stage, and then gradually decreased to 56.4 % after 72 h at $850^\circ C$. In contrast, the CeO_x -overcoated Ni/Al_2O_3 catalyst exhibited better stability and activity. Notably, all CeO_x -overcoated Ni/Al_2O_3 catalysts exhibited an activation process in the initial 5 h of reaction, which might be ascribed to the formation of $CeAlO_3$ and further reduction of $NiAl_2O_4$ to metallic Ni, as discussed in our previous work [40,44], and then a stable conversion could be reached. In this work, 60 cycles of CeO_x exhibited an optimal effect on the Ni/Al_2O_3 catalyst for the BRM reaction. The highest conversion at 87.2 % was achieved for the $60CeO_x-Ni/Al_2O_3$ catalyst due to the optimum loading of the CeO_2 overcoating with 60 cycles of CeO_2 ALD, which is much better than that of the uncoated, $10CeO_x-Ni/Al_2O_3$, $30CeO_x-Ni/Al_2O_3$, and $90CeO_2-Ni/Al_2O_3$ catalysts. In Fig. 5b, the H_2/CO of Ni/Al_2O_3 and CeO_x -overcoated Ni/Al_2O_3 reached ~ 2.05 , which is close to the value of 2 for the stoichiometric combination DRM/SMR with a feedstock ratio of $H_2O/CO_2/CH_4 = 2/1/3$.

Bi-reforming of methane with $H_2O/CO_2/CH_4=2/1/3$ was also tested at $750^\circ C$, as shown in Fig. 6. The deactivation of Ni/Al_2O_3 at $750^\circ C$ was more severe than the test at $850^\circ C$ using the same catalyst.

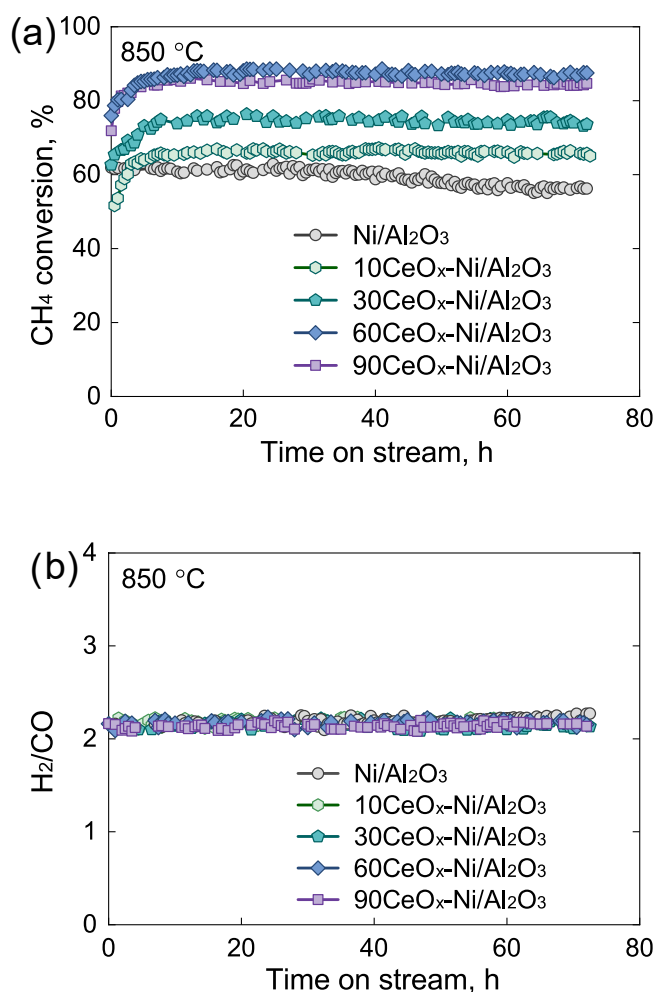


Fig. 5. (a) CH_4 conversion and (b) H_2/CO ratio of BRM as a function of time on stream using Ni/Al_2O_3 , $10CeO_x-Ni/Al_2O_3$, $30CeO_x-Ni/Al_2O_3$, $60CeO_x-Ni/Al_2O_3$, and $90CeO_x-Ni/Al_2O_3$. Reaction conditions: 50 mg catalyst, 30 mL/min CH_4 , 10 mL/min CO_2 , 20 mL/min H_2O (gas phase), at $850^\circ C$.

The CH_4 conversion for Ni/Al_2O_3 decreased from 39.4 % to 19.8 % in 72 h, which could be ascribed to the oxidation of the Ni surface and coke formation at a lower reaction temperature. The Al_2O_3 ALD overcoated Al_2O_3-Ni/Al_2O_3 catalyst and the CeO_2 IW promoted $iwCeO_2-Ni/Al_2O_3$ catalyst exhibited better stability than that of Ni/Al_2O_3 , but there was still gradual deactivation. In contrast, the CeO_x ALD overcoated $60CeO_x-Ni/Al_2O_3$ catalyst greatly enhanced the stability and activity for BRM, with a stable conversion at 53.5 % during a test of 150 h. As for the product, the H_2/CO ratio of BRM using the Ni/Al_2O_3 catalyst increased from 2.45 to 2.88, which could be ascribed to the limited water-gas shift reaction. For the $60CeO_x-Ni/Al_2O_3$ catalyst, the H_2/CO ratio was kept at ~ 2.34 . Therefore, the CeO_x ALD overcoating successfully decorated the Ni sites and enhanced the catalytic performance due to its high oxygen vacancy properties and sufficient Ni- CeO_x interface.

The catalytic behavior of uncoated Ni/Al_2O_3 and $60CeO_x-Ni/Al_2O_3$ for methane reforming was systematically tested at different temperatures. Fig. 7 depicts the CH_4 conversion and H_2/CO molar ratio for BRM with an inlet feed of $H_2O/CO_2/CH_4 = 2/1/3$ at different temperatures. In Fig. 7a, the enhanced activity was observed for $60CeO_x-Ni/Al_2O_3$ at varying temperatures, verifying the promoting effects of CeO_x ALD overcoating. In Fig. 7b, the H_2/CO ratio for uncoated Ni/Al_2O_3 and $60CeO_x-Ni/Al_2O_3$ was higher than the value based on the stoichiometric combination (i.e., $H_2/CO = 2$) or the equilibrium ratio, especially at low temperatures. On one hand, the deviation between the practical H_2/CO ratio of BRM products and the equilibrium H_2/CO ratio might be explained by the severe water gas shift reaction. On the other hand, BRM is based on the catalytic dissociation of CH_4 on Ni sites and the following oxidation by H_2O or CO_2 , so the H_2/CO ratio in the products should be directly related to the activation process of H_2O or CO_2 . Therefore, the difference of H_2/CO ratio for the reaction catalyzed by Ni/Al_2O_3 and $60CeO_x-Ni/Al_2O_3$ indicated that CeO_x overcoating could affect the reactant activation. Therefore, the lower H_2/CO ratio for $60CeO_x-Ni/Al_2O_3$ indicated that the CeO_x overcoating could have a better capability in CO_2 activation, which was ascribed to the oxygen vacancies of CeO_x ALD.

Fig. 8 shows the catalytic performance of uncoated Ni/Al_2O_3 and $60CeO_x-Ni/Al_2O_3$ at $750^\circ C$ and $850^\circ C$ with different ratios of $H_2O/CO_2/CH_4$ but $(H_2O + CO_2)/CH_4 = 1$ in the feed as the combination of DRM and SRM. In Fig. 8a, the CeO_x ALD overcoating significantly enhanced the CH_4 conversion for $60CeO_x-Ni/Al_2O_3$, as compared to the uncoated Ni/Al_2O_3 under different feed conditions. For instance, the CH_4 conversion was 62.6 % for Ni/Al_2O_3 and 87.6 % for $60CeO_x-Ni/Al_2O_3$ with a feed of $H_2O/CO_2/CH_4 = 3/0/3$ (which is the case of SRM) at $850^\circ C$. Besides, it was noted that the H_2O/CO_2 ratio in the feed influenced the CH_4 conversion. For instance, the CH_4 conversion for $60CeO_x-Ni/Al_2O_3$ with feed $H_2O/CO_2/CH_4 = 0/3/3$ (which is the case of DRM) was 86.2 % at $850^\circ C$, and a higher CH_4 conversion was achieved with a higher H_2O content ratio in the feed, reaching CH_4 conversion of 87.2 % with a feed of $H_2O/CO_2/CH_4 = 2/1/3$, and 87.6 % with a feed of $H_2O/CO_2/CH_4 = 3/0/3$. The higher conversion for high-content H_2O in feed is more significant for Ni/Al_2O_3 , with CH_4 conversion at $750^\circ C$ reaching CH_4 conversion of 57.7 % with $H_2O/CO_2/CH_4 = 0/3/3$ (DRM), 62.1 % at $H_2O/CO_2/CH_4 = 2/1/3$, and 62.6 % at $H_2O/CO_2/CH_4 = 3/0/3$ (SRM). The influence of H_2O in the feed is more significant at lower temperatures. At $750^\circ C$, $60CeO_x-Ni/Al_2O_3$ had a CH_4 conversion of 47.9 % for DRM and 52.1 % for SRM, and Ni/Al_2O_3 had a CH_4 conversion of 32.7 % for DRM and 41.1 % for SRM, indicating that the effects of H_2O on CH_4 conversion were less significant for $60CeO_x-Ni/Al_2O_3$. The better performance with a higher H_2O content in the feed might be ascribed to the activation of CO_2 . The H_2/CO ratio at $850^\circ C$ for both catalysts was close to the equilibrium value, whereas the H_2/CO ratio at $750^\circ C$ was far from the equilibrium value, especially for Ni/Al_2O_3 . Similar to the previous discussion, the H_2/CO ratio might be affected by the water-gas shift reaction and the activation process for H_2O or CO_2 . It seems that the CeO_x overcoating could enhance the CO_2 activation and achieve a H_2/CO ratio which was close to the equilibrium

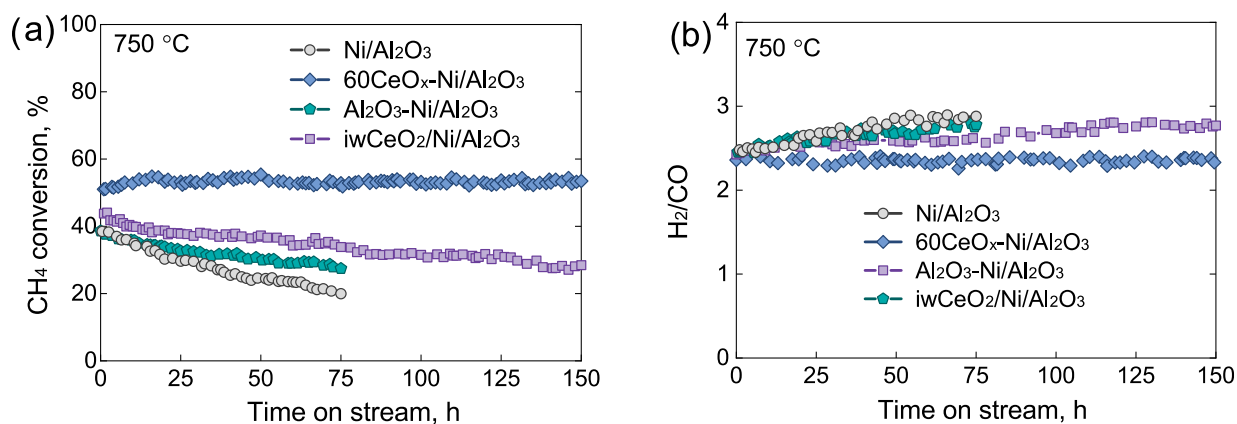


Fig. 6. (a) CH₄ conversion and (b) H₂/CO ratio of BRM as a function of time on stream using Ni/Al₂O₃, 60CeO_x-Ni/Al₂O₃, Al₂O₃-Ni/Al₂O₃, and iwCeO₂/Ni/Al₂O₃ as catalysts. Reaction conditions: 50 mg catalyst, 30 mL/min CH₄, 10 mL/min CO₂, and 20 mL/min H₂O (gas phase), and 750 °C.

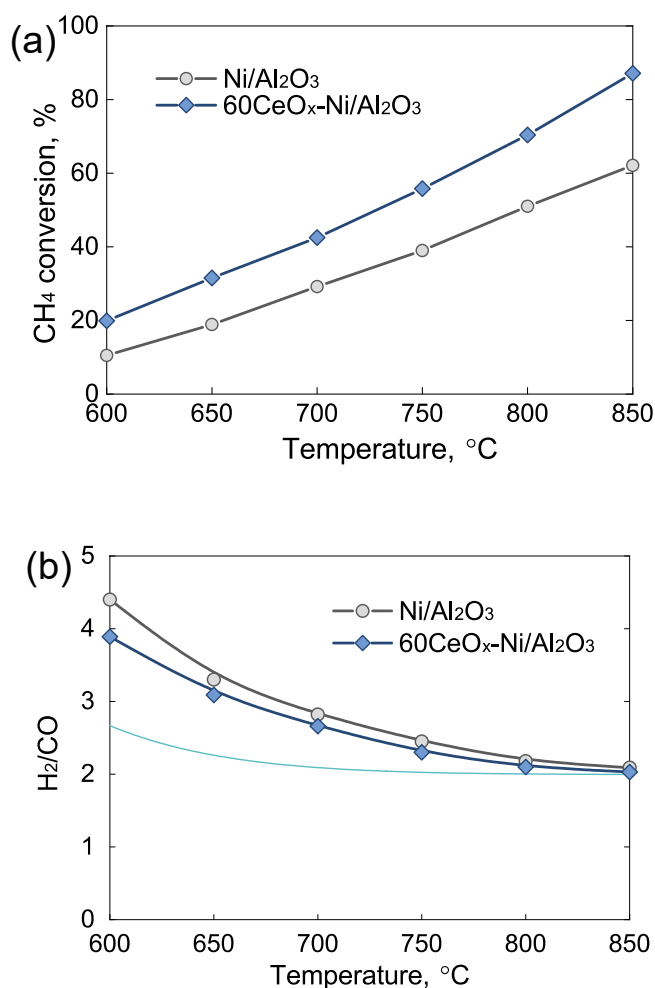


Fig. 7. (a) CH₄ conversion and (b) H₂/CO ratio of BRM as a function of reaction temperature using Ni/Al₂O₃ and 60CeO_x-Ni/Al₂O₃. Reaction conditions: 50 mg catalyst, 30 mL/min CH₄, 10 mL/min CO₂, and 20 mL/min H₂O (gas phase).

value.

H₂ pulse chemisorption was conducted to demonstrate the confinement effects and the promoting effects of CeO_x overcoating on Ni/Al₂O₃ for BRM reaction, as shown in Fig. 9. With the increase in the cycle number of CeO_x ALD overcoating, the Ni surface area exhibited a decreasing trend, which indicates that the CeO_x overcoating partially

covered the Ni surface and confined the Ni sites. The turnover frequency (TOF) was also calculated to investigate the intrinsic reaction activity with the order as follows: 90CeO_x-Ni/Al₂O₃ ≈ 60CeO_x-Ni/Al₂O₃ > 30CeO_x-Ni/Al₂O₃ > Ni/Al₂O₃. The increasing TOF value with the increase in the ALD cycle number indicates that the CeO_x overcoating enhanced the intrinsic reaction rate.

3.3. Characterizations of spent catalysts

The sintering of Ni NPs is generally one of the main reasons for catalyst deactivation. TEM was used to investigate the Ni NPs size for the spent catalysts in Fig. 10. For the spent Ni/Al₂O₃ catalyst in Fig. 10a, the average size for Ni NPs was 24.6 ± 5.2 nm. For the spent 60CeO_x-Ni/Al₂O₃ catalyst in Fig. 10b, the average size for Ni was 18.4 ± 3.8 nm. The presence of CeO_x ALD overcoating greatly prevented the mobilization of Ni NPs, possibly due to the Ni-CeO_x interaction or the geometric confinement effect of CeO_x coating [45], thus preventing the sintering of Ni NPs and enhancing the stability of the Ni NPs.

During SRM or DRM, the catalytic dissociation of methane on metal sites is generally considered as the initial step to generate H and CH_x (x = 0–3) and the oxidants (H₂O or CO₂) will undergo dissociation and activation for the oxidation of CH_x. However, the side reactions (CH₄ cracking and Boudouard reaction) share the same species as carbon intermediates in the elementary step and inevitably result in carbon growth [10,13]. During methane reforming, the carbon formation resulted from the side reactions and the low oxidation rate of coke by the reactants (i.e., H₂O and CO₂). To determine the carbon growth rate during the bi-reforming of methane, O₂-TPO was conducted on the spent catalysts. As shown in Fig. 11 a, spent Ni/Al₂O₃, spent 30CeO_x-Ni/Al₂O₃, spent 60CeO_x-Ni/Al₂O₃, and spent 90CeO_x-Ni/Al₂O₃ after bi-reforming of methane at 850 °C for 72 h (H₂O/CO₂/CH₄ = 2/1/3) were tested. The oxidation temperature of the surface carbon on these catalysts ranged from 300 to 750 °C, indicating different carbon species. According to the oxidation temperature, the chemical composition and crystallization of carbon can be determined. The carbon peak at < 400 °C was assigned to the carbidic carbon (C_α), the carbon peak at 400–600 °C was assigned to the amorphous carbon (C_β), and the carbon peak at > 600 °C was assigned to the graphitic carbon (C_γ) [46,47]. In this work, all three carbon species resulted from the bi-reforming of methane reaction, especially for the amorphous carbon and graphitic carbon. As for the catalysts with CeO_x ALD overcoating, there exhibited a great decrease in the carbon amount, mainly for the amorphous carbon and graphitic carbon. Studies showed that further graphitization growth was catalyzed on the large Ni NPs and insufficient oxidation rate. The CeO_x overcoating on Ni NPs made the Ni sites discontinuously exposed, then limited the graphitization growth. Besides, the oxygen sites on CeO_x, especially the oxygen vacancies, provided the activation sites for CO₂ or

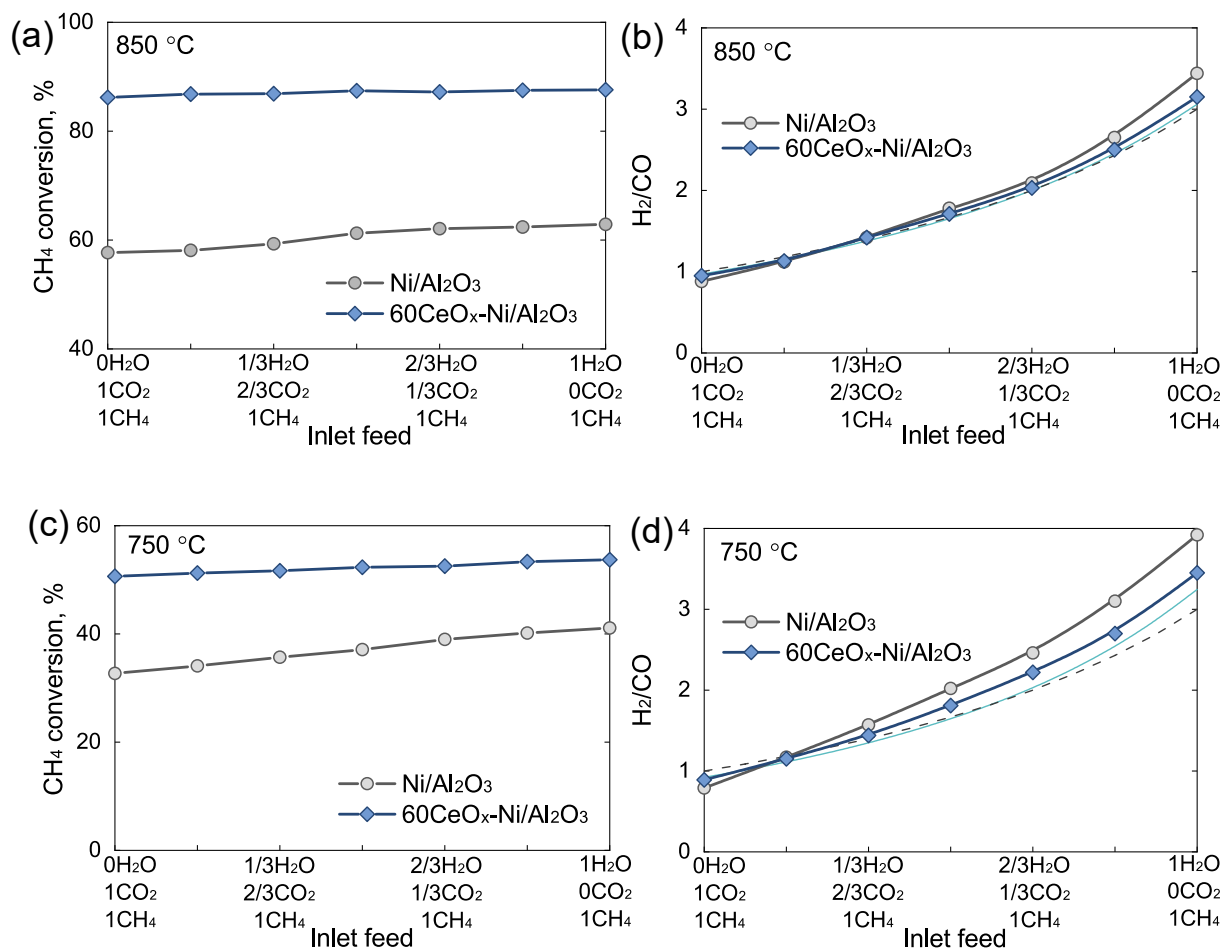


Fig. 8. (a) CH₄ conversion and (b) H₂/CO ratio of BRM as a function of feed conditions using Ni/Al₂O₃ and 60CeO_x-Ni/Al₂O₃ as catalysts at 850 °C. (c) CH₄ conversion and (d) H₂/CO ratio of BRM as a function of feed conditions using Ni/Al₂O₃ and 60CeO_x-Ni/Al₂O₃ as catalysts at 750 °C. Reaction conditions: 50 mg catalyst and inlet feed (H₂O + CO₂)/CH₄ = 1.

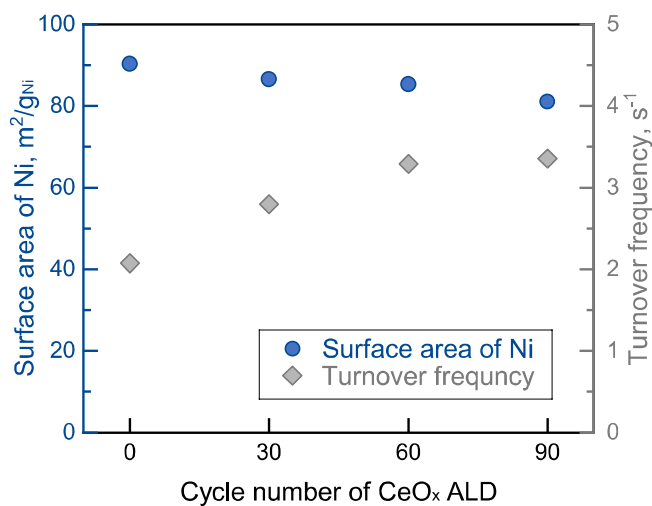


Fig. 9. Ni surface area based on H₂-chemisorption and turnover frequency of methane on Ni sites for bi-reforming of methane as the function of CeO_x ALD cycle number on Ni/Al₂O₃.

H₂O and enabled the high concentration of surface O for carbon oxidation. Therefore, a decreasing amount of carbon deposition was found with the increase in the number of CeO_x ALD cycles. TGA was also conducted to determine the carbon deposition on spent Ni/Al₂O₃ and

spent 60CeO_x-Ni/Al₂O₃, as shown in Fig. 11b. The catalysts first underwent a preheating process at 200 °C to remove any moisture. When the temperature ramped from 200 to 900 °C, the weight of Ni/Al₂O₃ decreased from 98.6 % to 96.5 %, indicating that 2.1 wt% coke was detected. Besides, the decrease at ~ 120 min indicates the existence of graphitic carbon. In comparison, the weight of 60CeO_x-Ni/Al₂O₃ decreased from 99.0 % to 98.2 %, indicating 0.8 wt% coke was detected. The lower coke amount was ascribed to the activation sites of H₂O and CO₂ on Ni-CeO_x interface. Therefore, the suppressing effects of CeO_x overcoating on coking was confirmed for Ni/Al₂O₃ in the methane reforming.

XPS spectra were collected using the spent Ni/Al₂O₃ and spent 60CeO_x-Ni/Al₂O₃ catalysts after bi-reforming of methane at 850 °C for 72 h, as shown in Fig. 12 and Fig. S6. For Ni 2p_{3/2}, there was 19.9 % NiAl₂O₄ for spent Ni/Al₂O₃ and 13.2 % NiAl₂O₄ for spent 60CeO_x-Ni/Al₂O₃. This indicates that the CeO_x overcoating enhanced the reducibility of NiAl₂O₄. Besides, it was noticed that there was more metallic Ni for the spent 60CeO_x-Ni/Al₂O₃ catalyst than that of spent Ni/Al₂O₃, which demonstrates that the CeO_x overcoating enhanced the reducibility and helped prevent the Ni nanoparticles from oxidation. The more metallic Ni sites by CeO_x overcoating means better utilization of Ni sites and better catalytic performance. Besides, for the O 1 s spectra, the 60CeO_x-Ni/Al₂O₃ catalyst still had a high amount of surface oxygen after the reaction process, indicating that the oxygen species of CeO_x overcoating was stable during the reaction.

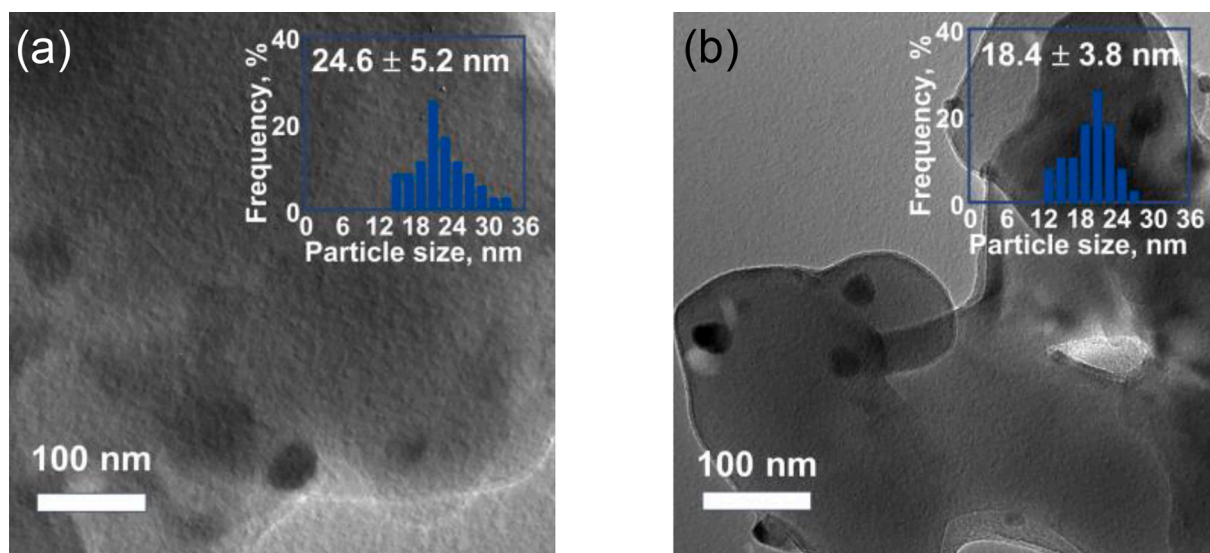


Fig. 10. TEM images of (a) spent Ni/Al₂O₃ and (b) spent 60CeO_x-Ni/Al₂O₃ after bi-reforming of methane reaction at 850 °C for 72 h. The inset images show the size distribution of Ni NPs.

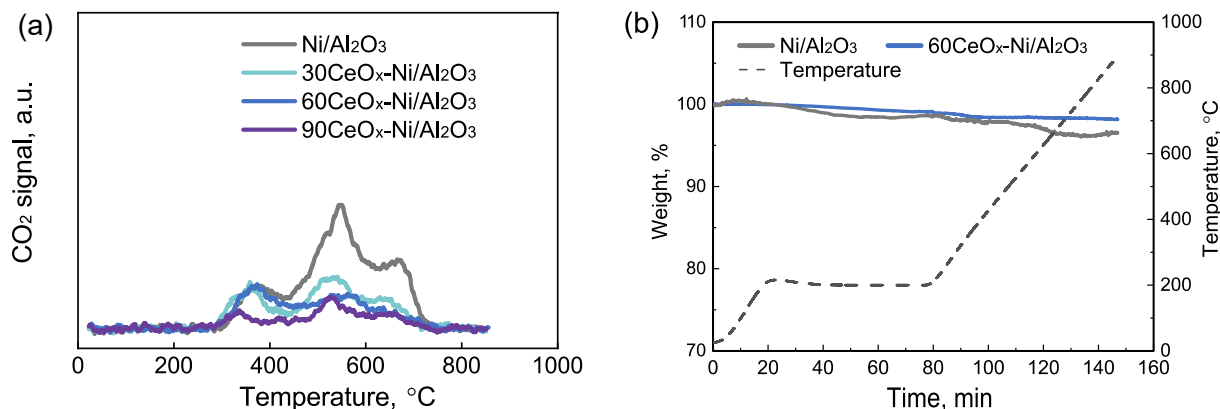


Fig. 11. (a) O₂-TPO of spent Ni/Al₂O₃, 30CeO_x-Ni/Al₂O₃, 60CeO_x-Ni/Al₂O₃, and 90CeO_x-Ni/Al₂O₃, (b) TGA of the spent Ni/Al₂O₃ and spent 60CeO_x-Ni/Al₂O₃. Spent catalysts underwent bi-reforming of methane at 850 °C for 72 h (H₂O/CO₂/CH₄ = 2/1/3).

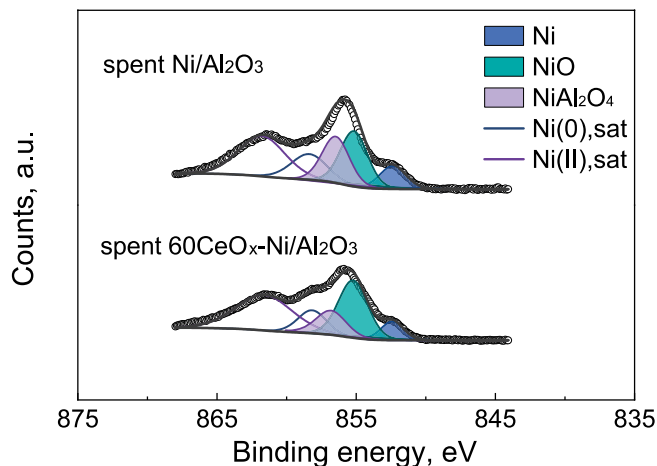


Fig. 12. XPS spectra of Ni 2p_{3/2} of spent Ni/Al₂O₃ and spent 60CeO_x-Ni/Al₂O₃ after bi-reforming of methane at 850 °C for 72 h (H₂O/CO₂/CH₄ = 2/1/3).

3.4. Mechanism of performance enhancement by CeO_x ALD overcoating

In this work, the effects of CeO_x ALD overcoating on Ni/Al₂O₃ for bi-reforming of methane was systematically studied. The mechanism of performance enhancement was proposed, as shown in Fig. S7. The CeO_x ALD overcoating was successfully deposited onto Ni/Al₂O₃ and a beneficial Ni-CeO_x interface was formed. The CeO_x ALD overcoating exhibited its unique chemical properties for enhanced performance as compared to the ALD Al₂O₃ or IW CeO₂ promoter. Compared to the lower reducibility of the Al₂O₃ ALD coated Ni/Al₂O₃ catalyst due to the formation of NiAl₂O₄ during Al₂O₃ ALD process, the CeO_x ALD overcoating greatly improved the reducibility of Ni(II) and prevented the oxidation of the active Ni NPs. Besides, CeO_x was oxygen-deficient in non-stoichiometric form, resulting in the high concentration of the oxygen vacancies. The high oxygen vacancies in CeO_x ALD overcoating provided higher activity in the CO₂ activation process and promoted the catalytic performance.

4. Conclusion

In this work, Ni/Al₂O₃ catalyst was prepared by depositing Ni NPs on Al₂O₃ NPs by ALD, followed by CeO_x ALD overcoating on Ni/Al₂O₃ catalyst with different numbers of cycles (i.e., 10, 30, 60, and 90). The

catalytic performance of CeO_x-Ni/Al₂O₃ was investigated for the bi-reforming of methane reaction. Based on TEM analysis, the Ni NPs size for the pristine Ni/Al₂O₃ catalyst was about 2.7 nm and the Ni size for the 60CeO_x-Ni/Al₂O₃ catalyst was about 2.9 nm, which indicates that the CeO_x ALD coating didn't change the morphology of Ni NPs due to its mild ALD temperature. Based on XPS and CO₂-TPD, CeO_x ALD overcoating was found to be in non-stoichiometric form with a high amount of Ce(III) and oxygen vacancies, which might be ascribed to the unique ALD growth process. Besides, the reduction process for the catalyst led to a further reduction of Ce(IV) to Ce(III) and generated more oxygen vacancies, which acted as the CO₂ activation sites and achieved a good balance between SRM and DRM. Based on TPR analysis, CeO_x ALD also enhanced the reducibility of Ni NPs and helped keep Ni in the metallic state. For the bi-reforming of methane, CeO_x ALD significantly improved the activity and stability and achieved a better control in the H₂/CO ratio at the designed H₂O/CO₂/CH₄ feed. For BRM at 850 °C with H₂O/CO₂/CH₄ = 2/1/3, which was intended to produce H₂/CO at 2, the CH₄ conversion was ~ 61.9 % for pristine Ni/Al₂O₃ and 87.2 % for 60CeO_x-Ni/Al₂O₃, with H₂/CO molar ratio at ~ 2.05 for both catalysts. For BRM at 750 °C with H₂O/CO₂/CH₄=2/1/3, the CH₄ conversion was ~ 39.4 % with gradual deactivation for pristine Ni/Al₂O₃ and ~ 53.5 % for 60CeO_x-Ni/Al₂O₃ in a 150-h test. Besides, the H₂/CO ratio varied from 2.45 to 2.88 for Ni/Al₂O₃ and kept stable at 2.34 for 60CeO_x-Ni/Al₂O₃ during a 75-h test. Under the varying H₂O/CO₂/CH₄ feed conditions (keeping (H₂O + CO₂)/CH₄ = 1), the 60CeO_x-Ni/Al₂O₃ catalyst exhibited a closer H₂/CO value to the direct stoichiometric combination result of SRM and DRM than that of the Ni/Al₂O₃ catalyst. Based on TPO results of spent catalysts, CeO_x ALD significantly decreased the carbon formation, especially the amorphous carbon and graphitic carbon, because CeO_x ALD overcoating could provide sufficient oxygen vacancies, which enhanced the oxidant activation to remove carbon intermediate and inhibited carbon formation.

Declaration of Competing Interest

The authors declare that they have no known competing financial interests or personal relationships that could have appeared to influence the work reported in this paper.

Data availability

Data will be made available on request.

Acknowledgment

This work was supported in part by the U.S. National Science Foundation (Award Number 2306177).

Appendix A. Supplementary data

Supplementary data to this article can be found online at <https://doi.org/10.1016/j.cej.2023.141611>.

References

- Y. Song, E. Ozdemir, S. Ramesh, A. Adishev, S. Subramanian, A. Harale, M. Albuali, B.A. Fadhel, A. Jamal, D. Moon, Dry reforming of methane by stable Ni–Mo nanocatalysts on single-crystalline MgO, *Science* 367 (2020) 777–781.
- D. Gielen, R. Gorini, N. Wagner, R. Leme, L. Gutierrez, G. Prakash, E. Amselash, L. Janeiro, G. Gallina, G. Vale, Global energy transformation: A roadmap to 2050 (2019).
- G.A. Olah, A. Goepfert, M. Czaun, G.S. Prakash, Bi-reforming of methane from any source with steam and carbon dioxide exclusively to metgas (CO–2H₂) for methanol and hydrocarbon synthesis, *J. Am. Chem. Soc.* 135 (2013) 648–650.
- G.A. Olah, A. Goepfert, M. Czaun, T. Mathew, R.B. May, G.S. Prakash, Single step bi-reforming and oxidative bi-reforming of methane (natural gas) with steam and carbon dioxide to metgas (CO–2H₂) for methanol synthesis: self-sufficient effective and exclusive oxygenation of methane to methanol with oxygen, *J. Am. Chem. Soc.* 137 (2015) 8720–8729.
- A. Saravanan, D.-V.-N. Vo, S. Jeevanantham, V. Bhuvaneshwari, V.A. Narayanan, P. Yaashikaa, S. Swetha, B. Reshma, A comprehensive review on different approaches for CO₂ utilization and conversion pathways, *Chem. Eng. Sci.* 116515 (2021).
- X. Fan, B. Jin, S. Ren, S. Li, M. Yu, X. Liang, Roles of interaction between components in CZZA/HZSM-5 catalyst for dimethyl ether synthesis via CO₂ hydrogenation, *AIChE J* 67 (2021) e17353.
- X. Fan, S. Ren, B. Jin, S. Li, M. Yu, X. Liang, Enhanced stability of Fe-modified CuO-ZnO-ZrO₂-Al₂O₃/HZSM-5 bifunctional catalysts for dimethyl ether synthesis from CO₂ hydrogenation, *Chin. J. Chem. Eng.* 38 (2021) 106–113.
- X. Yan, T. Hu, P. Liu, S. Li, B. Zhao, Q. Zhang, W. Jiao, S. Chen, P. Wang, J. Lu, Highly efficient and stable Ni/CeO₂-SiO₂ catalyst for dry reforming of methane: effect of interfacial structure of Ni/CeO₂ on SiO₂, *Appl Catal B* 246 (2019) 221–231.
- Y.-X. Pan, P. Kuai, Y. Liu, Q. Ge, C.-J. Liu, Promotion effects of Ga₂O₃ on CO₂ adsorption and conversion over a SiO₂-supported Ni catalyst, *Energ. Environ. Sci.* 3 (2010) 1322–1325.
- M. Akri, S. Zhao, X. Li, K. Zang, A.F. Lee, M.A. Isaacs, W. Xi, Y. Gangarajula, J. Luo, Y. Ren, Atomically dispersed nickel as coke-resistant active sites for methane dry reforming, *Nat. Commun.* 10 (2019) 1–10.
- B. Qi, O. Farid, A.F. Velo, J. Mendil, S. Uribe, Y. Kaneko, K. Sakakura, Y. Kagota, M. Al-Dahhan, Tracking the heavy metal contaminants entrained with the flow into a trickle bed hydrotreating reactor packed with different catalyst shapes using newly developed noninvasive dynamic radioactive particle tracking, *Chem. Eng. J.* 429 (2022), 132277.
- B. Qi, S. Uribe, O. Farid, M. Al-Dahhan, Development of a hybrid pressure drop and liquid holdup phenomenological model for trickle bed reactors based on two-phase volume averaged equations, *Can. J. Chem. Eng.* 99 (2021) 1811–1823.
- Y. Lou, M. Steib, Q. Zhang, K. Tiefenbacher, A. Horváth, A. Jentys, Y. Liu, J. A. Lercher, Design of stable Ni/ZrO₂ catalysts for dry reforming of methane, *J. Catal.* 356 (2017) 147–156.
- Y. Liu, Y. Wu, Z. Akhtamberdinova, X. Chen, G. Jiang, D. Liu, Dry reforming of shale gas and carbon dioxide with Ni-Ce-Al₂O₃ catalyst: syngas production enhanced over Ni-CeO_x formation, *ChemCatChem* 10 (2018) 4689–4698.
- X. Du, D. Zhang, L. Shi, R. Gao, J. Zhang, Morphology dependence of catalytic properties of Ni/CeO₂ nanostructures for carbon dioxide reforming of methane, *J. Phys. Chem. C* 116 (2012) 10009–10016.
- Z. Wang, Z. Huang, J.T. Brosnahan, S. Zhang, Y. Guo, Y. Guo, L. Wang, Y. Wang, W. Zhan, Ru/CeO₂ catalyst with optimized CeO₂ support morphology and surface facets for propane combustion, *Environ. Sci. Tech.* 53 (2019) 5349–5358.
- F. Jiang, S. Wang, B. Liu, J. Liu, L. Wang, Y. Xiao, Y. Xu, X. Liu, Insights into the influence of CeO₂ crystal facet on CO₂ hydrogenation to methanol over Pd/CeO₂ catalysts, *ACS Catal.* 10 (2020) 11493–11509.
- J. Vecchiotti, A. Bonivardi, W. Xu, D. Stacchiola, J.J. Delgado, M. Calatayud, S.N. E. Collins, Understanding the role of oxygen vacancies in the water gas shift reaction on ceria-supported platinum catalysts, *ACS Catal.* 4 (2014) 2088–2096.
- I. Luisetto, S. Tuti, C. Romano, M. Boaro, E. Di Bartolomeo, J.K. Kesavan, S. S. Kumar, K. Selvakumar, Dry reforming of methane over Ni supported on doped CeO₂: New insight on the role of dopants for CO₂ activation, *J. CO₂ Util.* 30 (2019) 63–78.
- L. Cao, J. Lu, Atomic-scale engineering of metal-oxide interfaces for advanced catalysis using atomic layer deposition, *Catal. Sci. Technol.* 10 (2020) 2695–2710.
- L. Cao, W. Liu, Q. Luo, R. Yin, B. Wang, J. Weissenrieder, M. Soldemo, H. Yan, Y. Lin, Z. Sun, Atomically dispersed iron hydroxide anchored on Pt for preferential oxidation of CO in H₂, *Nature* 565 (2019) 631–635.
- X. Wang, B. Jin, Y. Jin, T. Wu, L. Ma, X. Liang, Supported single Fe atoms prepared via atomic layer deposition for catalytic reactions, *ACS Appl. Nano Mater.* 3 (2020) 2867–2874.
- X. Wang, C. Zhang, B. Jin, X. Liang, Q. Wang, Z. Zhao, Q. Li, Pt–Carbon interaction-determined reaction pathway and selectivity for hydrogenation of 5-hydroxymethylfurfural over carbon supported Pt catalysts, *Catal. Sci. Technol.* 11 (2021) 1298–1310.
- H. Yan, K. He, I.A. Samek, D. Jing, M.G. Nanda, P.C. Stair, J.M. Notesstein, Tandem In₂O₃-Pt/Al₂O₃ catalyst for coupling of propane dehydrogenation to selective H₂ combustion, *Science* 371 (2021) 1257–1260.
- J. Lu, B. Fu, M.C. Kung, G. Xiao, J.W. Elam, H.H. Kung, P.C. Stair, Coking-and sintering-resistant palladium catalysts achieved through atomic layer deposition, *Science* 335 (2012) 1205–1208.
- Z. Shang, X. Liang, “Core-shell” nanostructured supported size-selective catalysts with high catalytic activity, *Nano Lett.* 17 (2017) 104–109.
- Z. Lu, R.W. Tracy, M.L. Abrams, N.L. Nicholls, P.T. Barger, T. Li, P.C. Stair, A. A. Dameron, C.P. Nicholas, C.L. Marshall, Atomic layer deposition overcoating improves catalyst selectivity and longevity in propane dehydrogenation, *ACS Catal.* 10 (2020) 13957–13967.
- T.M. Onn, S. Zhang, L. Arroyo-Ramirez, Y.-C. Chung, G.W. Graham, X. Pan, R. J. Gorte, Improved thermal stability and methane-oxidation activity of Pd/Al₂O₃ catalysts by atomic layer deposition of ZrO₂, *ACS Catal.* 5 (2015) 5696–5701.
- B. Jin, S. Li, Y. Liu, X. Liang, Engineering metal-oxide interface by depositing ZrO₂ overcoating on Ni/Al₂O₃ for dry reforming of methane, *Chem. Eng. J.* 436 (2022), 135195.
- K. Yuan, Q. Cao, H.-L. Lu, M. Zhong, X. Zheng, H.-Y. Chen, T. Wang, J.-J. Delaunay, W. Luo, L. Zhang, Oxygen-deficient WO_{3-x}@TiO_{2-x} core-shell nanosheets for efficient photoelectrochemical oxidation of neutral water solutions, *J. Mater. Chem. A* 5 (2017) 14697–14706.
- X. Liang, L.F. Hakim, G.D. Zhan, J.A. McCormick, S.M. George, A.W. Weimer, J. A. Spencer, K.J. Buechler, J. Blackson, C.J. Wood, Novel processing to produce

- polymer/ceramic nanocomposites by atomic layer deposition, *J. Am. Ceram. Soc.* 90 (2007) 57–63.
- [32] G. Pantaleo, V. La Parola, F. Deganello, R. Singha, R. Bal, A. Venezia, Ni/CeO₂ catalysts for methane partial oxidation: synthesis driven structural and catalytic effects, *Appl Catal B* 189 (2016) 233–241.
- [33] R.-P. Ye, Q. Li, W. Gong, T. Wang, J.J. Razink, L. Lin, Y.-Y. Qin, Z. Zhou, H. Adidharma, J. Tang, High-performance of nanostructured Ni/CeO₂ catalyst on CO₂ methanation, *Appl Catal B* 268 (2020), 118474.
- [34] A. Gupta, T.S. Sakthivel, C.J. Neal, S. Koul, S. Singh, A. Kushima, S. Seal, Antioxidant properties of ALD grown nanoceria films with tunable valency, *Biomater. Sci.* 7 (2019) 3051–3061.
- [35] J. Liu, L.R. Redfern, Y. Liao, T. Islamoglu, A. Atilgan, O.K. Farha, J.T. Hupp, Metal–organic-framework-supported and-isolated ceria clusters with mixed oxidation states, *ACS Appl. Mater. Interfaces* 11 (2019) 47822–47829.
- [36] J.W. Shin, S. Oh, S. Lee, D. Go, J. Park, H.J. Kim, B.C. Yang, G.Y. Cho, J. An, ALD CeO₂-Coated Pt anode for thin-film solid oxide fuel cells, *Int. J. Hydrogen Energy* 46 (2021) 20087–20092.
- [37] M. Zhang, J. Zhang, Y. Wu, J. Pan, Q. Zhang, Y. Tan, Y. Han, Insight into the effects of the oxygen species over Ni/ZrO₂ catalyst surface on methane reforming with carbon dioxide, *Appl Catal B* 244 (2019) 427–437.
- [38] B. Jin, S. Li, X. Liang, Enhanced activity and stability of MgO-promoted Ni/Al₂O₃ catalyst for dry reforming of methane: role of MgO, *Fuel* 284 (2021), 119082.
- [39] R. Yang, C. Xing, C. Lv, L. Shi, N. Tsubaki, Promotional effect of La₂O₃ and CeO₂ on Ni/ γ -Al₂O₃ catalysts for CO₂ reforming of CH₄, *Appl. Catal. A* 385 (2010) 92–100.
- [40] B. Jin, Z. Shang, S. Li, Y.-B. Jiang, X. Gu, X. Liang, Reforming of methane with carbon dioxide over cerium oxide promoted nickel nanoparticles deposited on 4-channel hollow fibers by atomic layer deposition, *Catal. Sci. & Technol.* 10 (2020) 3212–3222.
- [41] A. Ruiz Puigdollers, P. Schlexer, S. Tosoni, G. Pacchioni, Increasing oxide reducibility: the role of metal/oxide interfaces in the formation of oxygen vacancies, *ACS Catal.* 7 (2017) 6493–6513.
- [42] J.L. Ewbank, L. Kovarik, F.Z. Diallo, C. Sievers, Effect of metal–support interactions in Ni/Al₂O₃ catalysts with low metal loading for methane dry reforming, *Appl. Catal. A* 494 (2015) 57–67.
- [43] X. Jia, X. Zhang, N. Rui, X. Hu, C.-J. Liu, Structural effect of Ni/ZrO₂ catalyst on CO₂ methanation with enhanced activity, *Appl Catal B* 244 (2019) 159–169.
- [44] B. Jin, S. Li, X. Liang, High-performance catalytic four-channel hollow fibers with highly dispersed nickel nanoparticles prepared by atomic layer deposition for dry reforming of methane, *Ind. Eng. Chem. Res.* 61 (2021) 10377–10386.
- [45] Y. Zhang, A. Chen, M.-W. Kim, A. Alaei, S.S. Lee, Nanoconfining solution-processed organic semiconductors for emerging optoelectronics, *Chem. Soc. Rev.* 50 (2021) 9375–9390.
- [46] L. Li, S. He, Y. Song, J. Zhao, W. Ji, C.-T. Au, Fine-tunable Ni@ porous silica core–shell nanocatalysts: synthesis, characterization, and catalytic properties in partial oxidation of methane to syngas, *J. Catal.* 288 (2012) 54–64.
- [47] L. Chen, Y. Lu, Q. Hong, J. Lin, F. Dautzenberg, Catalytic partial oxidation of methane to syngas over Ca-decorated-Al₂O₃-supported Ni and NiB catalysts, *Appl. Catal. A* 292 (2005) 295–304.